ELSEVIER

Calculated signal-to-noise ratio of MRI detected with SQUIDs and Faraday detectors in fields from 10 µT to 1.5 T

Whittier Myers [a], Daniel Slichter [a], Michael Hatridge [a], Sarah Busch [a], Michael Mößle [a], Robert McDermott [a,1], Andreas Trabesinger [b,2], John Clarke [a,*]

[a] *Department of Physics, University of California, Berkeley, and Materials Sciences Division, Lawrence Berkeley National Laboratory, CA 94720, USA*
[b] *Department of Chemistry, University of California, Berkeley, and Materials Sciences Division, Lawrence Berkeley National Laboratory, CA 94720, USA*

Abstract

We examine the calculated signal-to-noise ratio (SNR) achievable with different MRI detection modalities in precession fields ranging from 10 µT to 1.5 T. In particular, we compare traditional Faraday detectors with both tuned and untuned detectors based on superconducting quantum interference devices (SQUIDs). We derive general expressions for the magnetic field noise due to the samples and the detectors, and then calculate the SNR achievable for a specific geometry with each modality with and without prepolarization. We show that each of the three modalities is superior in one of the three field ranges. SQUID-based detection is superior to conventional Faraday detection for MRI in precession fields below 250 mT for a 65 mm diameter surface coil placed a distance of 25 mm from the voxel of interest embedded in a cylinder of tissue 50 mm tall and of radius 50 mm. This crossover field, however, is sensitive to the geometry.
© 2007 Elsevier Inc. All rights reserved.

Keywords: Magnetic resonance imaging; SQUID; Signal-to-noise ratio; Tuned detection; Untuned detection

1. Introduction

Clinical MR images demand a high signal-to-noise ratio (SNR). The SNR of a conventional Faraday detector increases as the precession magnetic field increases, but there can be advantages to using a lower precession field. The benefits of MRI at lower fields include potentially reduced system costs and more open coil geometries [1,2], reduced susceptibility artifacts [3–5], and increased proton T_1 contrast between some tissues [6]. These benefits, however, must be balanced against the reduced SNR that generally accompanies low-field MRI. At low precession frequencies, the sample magnetization induced by the precession field B_0 may be insufficient to provide adequate SNR. The SNR can be increased by using a pulsed prepolarization field B_p greater than B_0, so that the initial sample magnetization is proportional to B_p and independent of B_0.

In this paper, we compare the performance of three MRI detection modalities at fields ranging from 10 µT to 1.5 T. In all cases, we represent the signal in terms of a magnetic field $B_{\mathrm{det}}(f)$ and the noise in terms of an equivalent magnetic field noise $S_B^{1/2}(f)$, both referred to the pickup loop of the detector. Consequently, the SNR scales as the sample magnetization divided by the equivalent magnetic field noise at the pickup loop per square root of frequency. In conventional Faraday detection, $|V(f)| = 2\pi f B_{\mathrm{det}}(f) A_p$ is the voltage induced in the pickup loop of area A_p from the magnetization precessing at frequency f. Therefore the equivalent magnetic field noise $S_B^{1/2}(f) = S_V^{1/2}(f)/2\pi f A_p$, where $S_V^{1/2}(f)$ is the Nyquist voltage noise from the resistive pickup loop. This concept of

---

equivalent magnetic field noise will allow us to more readily compare noise from different sources and the different detectors we will consider in this paper.

The relevant noise sources are the sample noise due to the Nyquist noise generated in conductive tissue and detector noise due to both Nyquist noise in the pickup coil and the noise of the signal amplifier. Since the sample noise is independent of detection modality, it sets a lower limit to the noise achievable at any given precession frequency. We have neglected external noise, for example environmental noise and any noise produced by magnetic field and gradient coils. At low frequencies—say below a few tens of kilohertz—environmental noise is generally high. Fortunately, this noise can be reduced substantially by using a gradiometer, rather than a magnetometer, as a detector.

As the precession frequency is decreased, the sample noise limit is more difficult to achieve using conventional detection with a room-temperature copper coil; at such frequencies, other detection modalities become beneficial. For example, Darasse and Ginefri [7] have reviewed the noise advantages of using cooled copper and high-temperature superconducting pickup coils in a conventional detector. Another option to reduce detector noise is to use tuned or untuned low-temperature superconducting pickup coils coupled to low-noise amplifiers based on superconducting quantum interference devices (SQUIDs), which are exquisitely sensitive to changes in magnetic flux. In this paper, we introduce the basics of SQUID detectors and compare their performance with that of room-temperature Faraday detectors.

A general comparison of the performance of these detection modalities is difficult because of the multitude of coil options and sample geometries. Since our primary interest is in the low field regime where cryogenically cooled pickup coils are necessary, we approach this problem from the point of view of the geometry available to us. Our current SQUID MRI system [8] is designed to look out from a liquid helium cryostat at an object of interest roughly 60 mm across. The pickup loop is a 65 mm diameter surface coil placed a distance d away from the voxel of inter-

est, as shown in Fig. 1, and is ideal for imaging joints or organs of similar dimension, for example the prostate. While we keep the size of the pickup loop fixed in this discussion, we aim to provide a useful resource for how to proceed with different coil sizes or regions of interest.

In Section 2, we calculate the oscillating magnetic field generated at the pickup coil by a voxel containing precessing protons, and estimate the noise from conducting tissue that sets the noise limit for all MRI detection modalities. Section 3 contains a description of the noise properties of SQUID amplifiers and calculations of the magnetic field noise of SQUID-based detectors with both tuned and untuned pickup coils. Section 4 briefly describes the magnetic field noise of Faraday detection using a room-temperature solid-wire copper coil. In Section 5, we plot the magnetic field noise of all three detection modalities as a function of frequency and compare the magnetic field noise to sample noise. We calculate the SNR of MRI using each of these detection modalities as a function of precession frequency. At precession fields below 100 mT, we use a 100 mT prepolarization field. We conclude in Section 6 by discussing the precession field range over which each of these techniques is optimal. The appendix contains a detailed derivation of the magnetic field noise in SQUID tuned detection.

2. Sample geometry and noise

The configuration of the sample and pickup coil is shown in Fig. 1. A voxel of volume $V_{voxel} = 1 \text{ mm}^3$ is embedded in a cylinder of sample tissue with radius R, height H and conductivity σ placed a distance h from the pickup coil, which has diameter $2a = 65$ mm; the voxel is at a distance d from the pickup coil. For SQUID-based detection we set $d = h = 25$ mm to account for the necessary separation of the pickup loop at 4.2 K from the signal source at body temperature. These dimensions are chosen to match those in Ref. [8]. For consistency, we choose the same dimensions for our calculations of conventional Faraday detection[3]. We calculate the magnetic field generated by the voxel and the noise generated by the conducting sample.

2.1. Magnetic field from a voxel of precessing spins

The amplitude of the magnetic field produced by the magnetization of the voxel can be found at the pickup loop using an electromagnetic principle of reciprocity [9] as

$$B_{det} = \frac{\mu_0 \beta_{receive,\perp}}{4\pi A_p} M V_{voxel}. \tag{1}$$

Here M is the voxel magnetization, $A_p = \pi a^2$ is the pickup coil area, and $\mu_0 \beta_{receive,\perp} /4\pi$ is the field perpendicular to
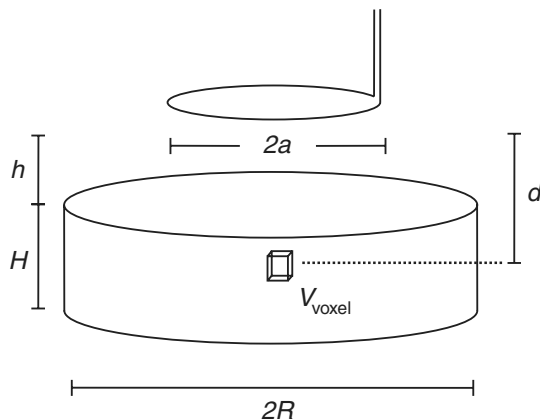

Fig. 1. Sample and pickup coil geometry.

---

[3] It turns out that for this geometry of pickup loop, the SNR of sample-noise-limited conventional detection is higher at $d = 25$ mm than at $d = 2$ mm. This fact is explained in greater detail in Section 5.

the plane of the pickup loop produced at the voxel per unit current flowing through the pickup loop. For the geometry shown in Fig. 1,

$$\beta_{receive,\perp} = 2\pi a^2/(a^2 + d^2)^{3/2}. \tag{2}$$

For spins in equilibrium at a polarizing field B_p and temperature T_S, we have $M = \rho\gamma^2\hbar^2 B_p/4k_B T_S$, where ρ is the spin density and $\gamma = 2.675 \times 10^8$ T^{-1} s^{-1} is the proton gyromagnetic ratio. Substituting for M and $\beta_{receive,\perp}$ in Eq. (1) yields

$$B_{det} = \frac{\mu_0}{4\pi} \frac{2V_{voxel}}{(a^2 + d^2)^{3/2}} \rho \frac{\gamma^2\hbar^2}{4k_B T_S} B_p = 9.0 \times 10^{-15} B_p, \tag{3}$$

where we have used $T_S = 310$ K and $\rho = 6.7 \times 10^{28}$ m^{-3}, the proton density of water. This equation demonstrates the inherently low-signal nature of MRI: applying a 1 T magnetic field to polarize the protons yields a signal of only 9 fT at the detector.

2.2. Sample noise

Since Nyquist noise in the conducting sample limits the ultimate sensitivity of all MRI detection modalities, it sets a useful scale for detector noise. Consequently, before calculating the detector noise for the various detection schemes, we estimate the magnetic field noise generated by the sample. Because capacitively coupled noise from the sample can be neglected at low frequencies and reduced through coil engineering at high frequencies [10], we consider only magnetically coupled noise. Our derivation follows that of Suits et al. [11], but extends their results to calculate the noise from cylinders of finite radius.

Their derivation begins by calculating the electrical power dissipated in the sample from the oscillating field generated by a current $I\sin\omega t$ flowing in the pickup coil. The time-averaged dissipated power can be expressed as an integral over the sample volume V

$$P_{loss}(\omega) = \frac{1}{2}\sigma\omega^2 \int_V \mathbf{A} \cdot \mathbf{A}\, d\mathbf{r}, \tag{4}$$

where $\mathbf{A}$ is the vector potential in the Coulomb gauge resulting from a static current I in the pickup coil and σ is the sample conductivity. This expression assumes the wavelength is much longer than the sample and detector sizes. If the sample is cylindrically symmetric about the pickup coil axis, the changing magnetic field produced by the circular pickup coil induces cylindrically symmetric currents in the sample and no electrical charge builds up. If, in addition, the sample is non-magnetic and much smaller than the skin depth, the vector potential in the sample can be approximated by its value in free space. For a circular loop of radius a in the $z = 0$ plane centered at the origin and carrying a current I,

$$\mathbf{A} = \frac{1}{2}\mu_0 Ia\hat{\mathbf{a}}_\theta \int_0^\infty e^{-k|z|}J_1(kr)J_1(ka)\, dk, \tag{5}$$

where $\hat{\mathbf{a}}_\theta$ is the azimuthal unit vector. To calculate the power lost in the sample shown in Fig. 1, we substitute Eq. (5) into Eq. (4) and integrate over the cylindrical volume. After integrating over the azimuthal coordinate and substituting $\lambda = ka$, we obtain

$$P_{loss}(\omega) = \frac{1}{4}\pi\sigma\mu_0^2 I^2\omega^2$$
$$\times \int_0^R \int_h^{h+H} r\left(\int_0^\infty e^{-\lambda|z|/a}J_1(\lambda r/a)J_1(\lambda)\, d\lambda\right)^2 dz\, dr$$
$$= \frac{1}{2}\sigma\mu_0^2 I^2\omega^2 V_{loss}, \tag{6}$$

where we have lumped all the geometrical factors into a single volume V_{loss}. This power is equivalent to a series resistance

$$R_S = P_{loss}/I_{rms}^2 = 2P_{loss}/I^2 = \sigma\mu_0^2\omega^2 V_{loss} \tag{7}$$

in the pickup coil, where I_{rms} is the root mean square current flowing in the pickup coil.

We refer all signal and noise quantities to the average magnetic field threading the pickup coil. Since the voltage noise in a coil with resistance R_i at temperature T produces a magnetic field noise $S_B^{1/2}(f) = \sqrt{4k_B T R_i}/\omega A_p$, where A_p is the pickup coil area, the magnetic field noise produced by the effective resistance R_S of the sample is

$$S_B^{1/2}(f) = \mu_0\sqrt{4k_B T_S\sigma V_{loss}}/A_p. \tag{8}$$

Here, $S_B(f)$ is the spectral density of the magnetic field noise per Hertz.

Gabriel et al. [12] have measured σ for biological tissue at frequencies f ranging from 10 Hz to 10 GHz. For tissue at the precession frequencies considered in this paper, they find σ to vary from 0.05 to 1.0 $(\Omega$ m$)^{-1}$ depending on frequency and tissue type. For all tissue types, the conductivity increases gradually with frequency. For simplicity, we assume that $\sigma(f)$ can be interpolated using a power law $\sigma = Af^B$ between $\sigma(1$ kHz$) = 0.1$ $(\Omega$ m$)^{-1}$ and $\sigma(10$ MHz$) = 0.5$ $(\Omega$ m$)^{-1}$; we determine $A = 0.0299$ and $B = 0.1747$. To evaluate Eq. (8), we integrate Eq. (6) numerically to find V_{loss} in the case of an infinite planar sample and two cylinders approximating a torso and an arm, respectively. Table 1 shows the noise in each case assuming $\sigma = 0.5$ $(\Omega$ m$)^{-1}$.

3. SQUID detection

3.1. SQUID amplifier fundamentals

The dc SQUID consists of a microfabricated thin-film washer of superconducting niobium interrupted by two Josephson junctions [13] (Fig. 2a). An input coil with N_i

Table 1
Sample noise evaluated with $h = 25$ mm, $T_S = 310$ K, and $\sigma = 0.5$ $(\Omega$ m$)^{-1}$

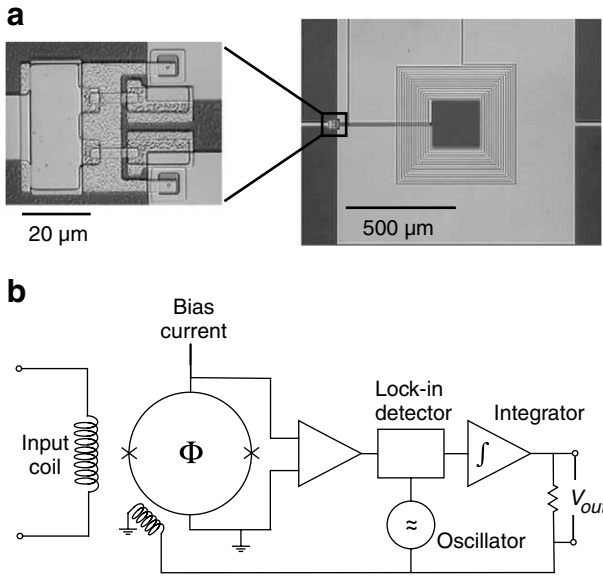| Model	R (m)	H (m)	V_{loss} (m^3)	$S_B^{1/2}$ (fT Hz$^{-1/2}$)
Half-plane	∞	∞	3.8×10^{-6}	0.068
"Torso"	0.2	0.2	2.6×10^{-6}	0.056
"Arm"	0.05	0.05	0.6×10^{-6}	0.027

Fig. 2. The dc SQUID. (a) Photographs of a thin-film SQUID with a multiturn input coil deposited on the washer with an intervening insulating layer. The expanded view shows the two Josephson junctions and resistive shunts. (b) Schematic of a SQUID connected to a flux-locked loop. The symbol "X" represents a Josephson junction.

turns deposited on the washer over an intervening insulating layer converts an input current to a flux through the SQUID. In the presence of a bias current, the voltage V across the SQUID is a periodic function of the flux Φ threading the washer; the period is the flux quantum $\Phi_0 \equiv h/2e \approx 2.07 \times 10^{-15}$ T m^2. We denote the maximum slope of the voltage versus flux curve as $V_\Phi \equiv |\partial V/\partial \Phi|_{max}$. The flux-locked loop shown in Fig. 2b produces an output voltage V_{out} linear in the current applied to the input coil. In practice, for room temperature electronics, it is difficult to operate the flux-locked loop at frequencies much above 10 MHz.

For a SQUID with inductance L, the input coil inductance is $L_i = \alpha^2 N_i^2 L$ and the mutual inductance between the input coil and SQUID is $M_i = \alpha^2 N_i L$, where α is the coupling coefficient. Simulations [14] show that for an optimized device there is a voltage noise V_N with spectral

density $S_V(f) \approx 16 k_B T R$ across the SQUID terminals and circulating current noise J_N with spectral density $S_J(f) \approx 11 k_B T/R$ around the SQUID loop; here R is the resistance shunting each junction. The voltage and current noises are partially correlated with cross-spectral density $S_{VJ}(f) \approx 12 k_B T$. The same simulations show that $V_\Phi \approx R/L$. Experimentally, these spectral densities have been shown to be frequency-independent for frequencies up to at least 5 GHz [15].[4]

We estimate the SNR of SQUID-detected MRI using measured parameters of the SQUID currently installed in our MRI system, for which $N_i = 60$, $L = 400$ pH, $L_i = 1.2$ μH, $M_i = 20$ nH, $R = 12$ Ω, and $T = 4.2$ K. For these parameters, the theory predicts $V_\Phi = 3.0 \times 10^{10}$ s^{-1}, voltage noise $S_V^{1/2}(f) = 0.11$ nV Hz$^{-1/2}$, and current noise $S_J^{1/2}(f) = 7.3$ pA Hz$^{-1/2}$.

3.2. Tuned and untuned magnetometers and gradiometers

To detect a magnetic field signal using a SQUID, one connects a superconducting pickup loop across the SQUID input coil. This circuit can be configured for either untuned or tuned detection. In untuned detection [8,17], the input coil of the SQUID and the pickup loop form a continuous superconducting loop that operates on the principle of flux conservation. This scheme measures magnetic flux rather than its rate of change, and its sensitivity is independent of frequency. Fig. 3a shows schematically an untuned magnetometer with a single-turn pickup coil of inductance L_p and area A_p. A superconducting shield encloses the SQUID to isolate it from external magnetic field fluctuations. Tuned detection [18,19] employs a capacitor in series with the inductances of the pickup and input coils, thereby eliminating their reactance at the resonant frequency. Fig. 3b shows a tuned magnetometer with a capacitance C_i inserted in the pickup loop. The resistor R_i represents a combination of eddy current losses in the cryostat, dielectric loss in the capacitor at the resonant frequency, and any intentionally added resistance. The pickup loop considered in this paper consists of a superconducting wire with a diameter $2\phi = 75$ μm. The calculated inductance is $L_p = \mu_0 a[\ln(8a/\phi) - 2] = 0.28$ μH [20].

In most SQUID applications, one replaces the magnetometers shown in Fig. 3 with superconducting gradiometers to reduce external magnetic noise. Since magnetic field gradients fall off more rapidly with distance than the corresponding magnetic fields, gradiometers discriminate against distant noise sources [21], including both environmental electromagnetic interference and Nyquist noise from tissue deep in the sample. In practice, for the SQUID
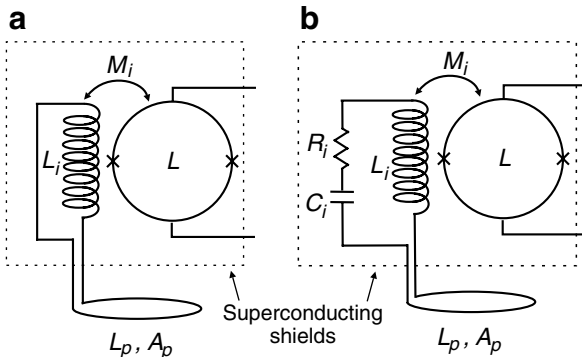

Fig. 3. SQUID magnetometers. (a) Schematic of a SQUID coupled to an untuned magnetometer. (b) Schematic of a SQUID coupled to a tuned magnetometer.

untuned detector at low frequencies, the sample noise is much lower than the detector noise (as will be shown in the latter part of this section), so that gradiometers are designed mainly to reject external environmental noise rather than sample noise. Such a gradiometer configuration has minimal impact on the signal. For this reason we assume a geometry with a baseline similar to the loop diameter. Fig. 4a shows a first-order axial gradiometer of baseline b with the bottom loop a distance d above the voxel of interest; the counter-wound top and bottom loops ensure that no current flows in response to a uniform applied field. Fig. 4b shows a second-order axial gradiometer that reduces external noise even more effectively. For $d \ll b$, we can neglect the response of the upper loop to the voxel magnetization and calculate the signal as if the device were a magnetometer, since the effect on $\beta_{\text{receive},\perp}$ in our gradiometer configuration is small ($\sim$10%) for distances less than one baseline. The sample noise is also decreased, especially if the dimensions of the gradiometer are such that the sample is many baselines deep. For the geometries considered in this paper, a second order gradiometer reduces the noise from the arm by a factor of 1.2 and the torso by 1.5. At low frequencies, however, the sample noise is negligible compared to the detector noise and therefore has no impact on the overall system noise of either magnetometers or gradiometers. At high fields where the sample noise limit is achievable, gradiometric operation is no longer the preferred modality. For ease of comparison across a wide range of parameters, therefore, we do not consider effects of gradiometers on the detected sample noise.

3.3. Magnetic field noise of SQUID untuned detection

In SQUID untuned detection, the input coil is noiseless at the detection frequency, and the noise is determined by the SQUID amplifier itself. A magnetic field B_{det} applied to the pickup coil of the SQUID untuned magnetometer shown in Fig. 3a causes a supercurrent $B_{\text{det}}A_p/L_T$ to flow in the input coil, where $L_T = L_i + L_p$. This in turn couples a flux $B_{\text{det}}A_p M_i/L_T$ into the SQUID, producing a voltage

Fig. 4. Superconducting axial gradiometers. (a) First-order. (b) Second-order. The arrows indicate the winding sense of each loop.

response $V_\Phi B_{\text{det}} A_p M_i / L_T$. Dividing the flux by the applied field yields the effective area

$$A_{\text{eff}} = A_p M_i / L_T = \alpha^2 N_i L A_p / (\alpha^2 N_i^2 L + L_p), \qquad (9)$$

where M_i and L_i have been evaluated for an N_i-turn input coil. The effective area is maximized when $N_i = (L_p/L)^{1/2}/\alpha$, which yields $L_i = L_p$. Replacing the single-turn pickup loop with an N_p-turn pickup loop increases the area by a factor of N_p and the inductance by a factor of N_p^2, leaving the effective area the same. Because a SQUID has fewer parasitic resonances when the number of turns on the input coil is reduced, untuned detection generally involves a single-turn pickup coil, enabling one to optimize the noise with the minimum number of turns on the input coil. In the simplest noise model, one neglects the circulating current noise of the SQUID and assumes that the magnetic field noise is determined by the voltage noise of the SQUID:

$$S_B^{1/2}(f) = \frac{1}{A_{\text{eff}} V_\Phi} S_V^{1/2}(f) = \frac{L_i + N_p^2 L_p}{N_p A_p M_i V_\Phi} S_V^{1/2}(f). \qquad (10)$$

Evaluating Eq. (10) for the pickup coil parameters of Section 3.2 and the SQUID parameters of Section 3.1 but allowing the number of input coil turns to vary yields $N_i = 29$ turns and $S_B^{1/2}(f) = 0.064\,\text{fT Hz}^{-1/2}$ for the untuned magnetometer. A second order gradiometer, which consists of two closely spaced loops and two distant loops, has an inductance of $6\,L_p$. From Eq. (10), this geometry yields $N_i = 60$ turns and $S_B^{1/2}(f) = 0.16\,\text{fT Hz}^{-1/2}$. More complicated models [22] that account for current noise and its partial correlation with the voltage noise predict 20–40% lower magnetic field noise.

3.4. Magnetic field noise of SQUID tuned detection

To perform SQUID-based tuned MRI detection, one inserts a tuning capacitor C_i and total resistance R_i in series with the input coil as shown in Fig. 3b. For this modality, we consider the noise of both the input circuit and the SQUID. To achieve low noise, the tuning capacitor must have a very high quality factor $Q_0 = 1/\omega C_i R_d$, where R_d represents the real part of the impedance due to dielectric losses at angular frequency ω. It appears that the largest practicable low-loss cryogenic lead/PFTE tuning capacitor would have a capacitance of 0.1 μF, placing an upper bound on the possible tuning capacitance [H. Seton, personal communication]. At the other extreme, stray capacitance in the pickup and input coils and leads can be several tens of picofarads, so we assume a minimum tuning capacitance of 100 pF. This ensures that the tuning capacitance dominates any stray capacitance. The tuning frequency can be adjusted by changing the tuning capacitance, the number of turns on the pickup and input coils, or both.

Seton et al. [18], following Clarke [21], calculate the voltage response of the SQUID to an applied field $B(\omega)$ to be

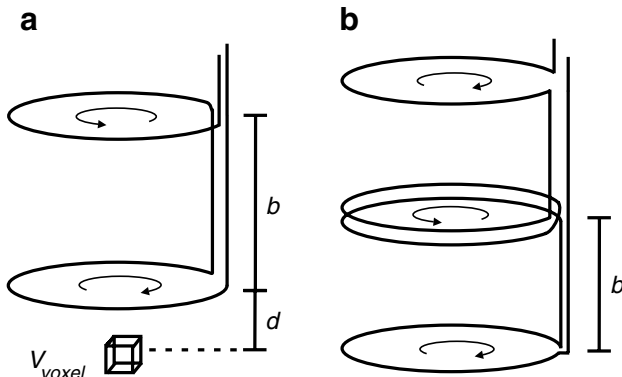$$V(\omega) = -j\omega M_i V_\Phi A_p B(\omega)/Z_T(\omega), \qquad (11)$$

where $Z_T(\omega) = R_i + j\omega L_T - j/\omega C_i$. We define an effective area for tuned detection, $A_{\mathrm{eff}} = A_p M_i \omega/|Z_T|$, from this expression. Since SQUID current noise becomes the dominant source of noise in SQUID tuned detection at high frequencies, we retain $S_J(f)$ in this case. Strictly speaking, we should also retain $S_{VJ}(f)$. However, the contribution of $S_{VJ}(f)$ vanishes on resonance [21], so to simplify the analysis we drop this term. The spectral density of the voltage noise across the SQUID is

$$S_V^{\mathrm{tot}}(f) = \frac{M_i^2 V_\Phi^2}{|Z_T|^2} 4k_B T R_i + S_V(f) + \frac{\omega^2 M_i^4 V_\Phi^2}{|Z_T|^2} S_J(f). \tag{12}$$

Dividing Eq. (12) by $V_\Phi^2 A_{\mathrm{eff}}^2$, yields the spectral density of the magnetic field noise

$$S_B(f) = \frac{1}{A_p^2} \left[\frac{4k_B T R_i}{\omega^2} + \frac{|Z_T|^2}{\omega^2 M_i^2 V_\Phi^2} S_V(f) + M_i^2 S_J(f) \right]. \tag{13}$$

As written, this equation describes only a single-turn pickup coil. For the tuned input circuit, we extend the analysis to represent a pickup coil with N_p turns by replacing A_p with $A_p N_p$ and L_p with $N_p^2 L_p$, such that $L_T = N_p^2 L_p + L_i$, where L_i is the inductance of an input coil with N_i turns. We rewrite Eq. (13) as:

$$S_B(f) = \frac{1}{N_p^2 A_p^2} \left[\frac{4k_B T R_i}{\omega^2} + \frac{|Z_T|^2}{\omega^2 M_i^2 V_\Phi^2} S_V(f) + M_i^2 S_J(f) \right]. \tag{14}$$

The half-width-at-half-maximum (HWHM) bandwidth of the stored energy of the pickup circuit is $\Delta f = R_i/2\pi L_T$. Since the bandwidth and noise of the tuned detector can be traded off against each other, we minimize noise by choosing the smallest possible bandwidth consistent with MRI requirements. Performing frequency encoding on a sample of length $2a$ with resolution Δx and NMR linewidth δf requires a bandwidth $2a\delta f/\Delta x$. We assume that the detector must have twice this bandwidth to achieve a sufficiently flat frequency response in the MRI bandwidth. In the case of negligible magnetic field inhomogeneity, $\delta f = 1/\pi T_2$, where T_2 is the transverse spin relaxation time, and the required detector bandwidth can be written as

$$BW_{\mathrm{det}} = 4a/\pi T_2 \Delta x. \tag{15}$$

Inserting $\Delta f = BW_{\mathrm{det}}/2$ gives the required damping resistance $R_i = 4aL_T/T_2\Delta x$. For representative biological tissue with $T_2 = 60$ ms, $2a = 65$ mm, and $\Delta x = 1$ mm, and assuming a single-turn magnetometer with $L_p = 0.28$ μH, we find $BW_{\mathrm{det}} = 690$ Hz and $R_i = 3.6$ mΩ. Assuming that the eddy current and dielectric losses of the superconducting resonator do not provide sufficient damping, one must add damping to the circuit. The most straightforward way is to add cold resistance in series with the pickup coil. However, Eq. (14) shows that increasing R_i adds Nyquist noise to the circuit. One can demonstrate that once the number of pickup coil turns has been optimized for lowest noise, the

Nyquist noise from R_i is much greater than the SQUID noise for all frequencies at which one can use feedback.

To provide damping without introducing additional Nyquist noise, Seton et al. [18], following the lead of Simmonds et al. [23], apply feedback damping to the input coil. Fig. 5 shows their most recent circuit. To increase the bandwidth of the input circuit, they feed back the phase-shifted output of the flux-locked loop to cancel part of the flux in the pickup coil. This feedback damping introduces an effective resistance [18]

$$\Delta R_i = \omega M_i M_f V_\Phi G/R_f, \tag{16}$$

where R_f is the resistance in the feedback damping line, M_f is the mutual inductance between the pickup loop and the feedback damping coil, and G is the total gain of all amplification stages past the SQUID. The bandwidth becomes $\Delta\omega = (R_i + \Delta R_i)/L_T$. Because ΔR_i is included in Z_T but does not contribute noise, Eq. (14) can be rewritten as

$$S_B(f) = \frac{1}{N_p^2 A_p^2} \left\{ \frac{4k_B T R_i}{\omega^2} + \frac{L_T^2[(\Delta\omega)^2\omega^2 + (\omega^2 - \omega_0^2)^2]}{\omega^4 M_i^2 V_\Phi^2} S_V(f) + M_i^2 S_J(f) \right\}, \tag{17}$$

where $\omega_0/2\pi$ is the MRI frequency and we have substituted $C_i = (\omega^2 L_T)^{-1}$ and $R_i = \Delta\omega L_T$; we assume that the resonant frequency of the pickup circuit is equal to the MRI frequency.

In the appendix we minimize the magnetic field noise of the tuned circuit with feedback damping relative to N_p, and find the optimal number of pickup coil turns

$$\tilde{N}_p^2 = \frac{L_i}{L_p} \left[1 + \frac{4k_B T \omega_0}{Q_0 S_V(f)} \frac{M_i^2}{L_i} \left(\frac{V_\Phi}{\Delta\omega} \right)^2 + \left(\frac{M_i^2}{L_i} \right)^2 \left(\frac{V_\Phi}{\Delta\omega} \right)^2 \frac{\omega_0^2 S_J(f)}{S_V(f)} \right]^{1/2} \tag{18}$$

and minimum magnetic field noise

$$\tilde{S}_B^{1/2}(f) \approx \sqrt{\frac{4k_B T L_p}{A_p^2 \omega_0 Q_0}}, \tag{19}$$

where $Q_0 = 1/\omega_0 C_i R_d$ is the intrinsic quality factor of the capacitor C_i with resistance R_d due to dielectric losses measured at angular frequency ω_0.
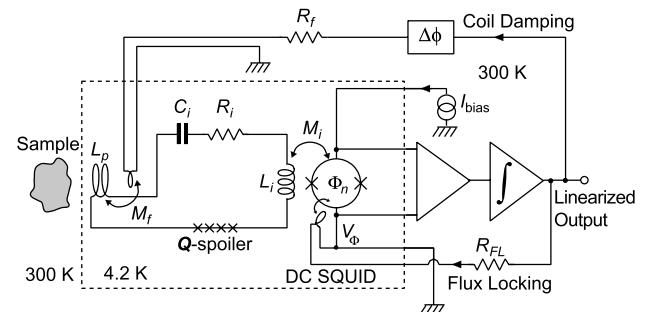

Fig. 5. Schematic of the tuned SQUID MRI system of Seton et al. showing the flux locked loop and feedback damping circuits. The Q-spoiler, which consists of a series array of Josephson junctions, damps the resonant circuit heavily during the application of large magnetic field pulses. Reproduced from [19] with permission.
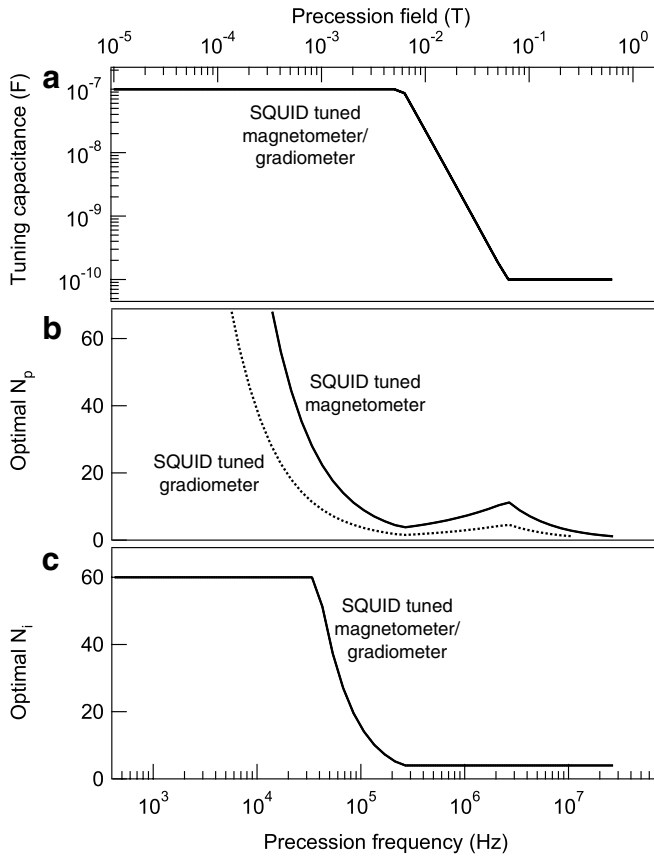
Fig. 6. Optimized parameters for SQUID tuned detection with a magnetometer or gradiometer. (a) Optimal tuning capacitance versus precession frequency. Note that at frequencies below 135 kHz and above 1.7 MHz, the tuning capacitance is limited by physical constraints. (b) Optimal number of pickup coil turns versus precession frequency. Below 50 kHz, N_p for a gradiometer is so large that it would be impractical to balance. (c) Optimal number of input coil turns versus precession frequency.

Fig. 6 plots N_p, N_i, and C_i versus precession frequency for tuned magnetometers and gradiometers. We generate this plot by first assuming $N_i = 4$ and calculating $\tilde{N}_p$ using Eq. (18); we choose $N_i = 4$ to yield reasonable values for $\tilde{N}_p$ and to keep the stripline capacitance of the input coil negligible.[5] If we cannot satisfy both the constraints on tuning capacitance and Eq. (18) with $N_i = 4$, we try increasing N_i, up to a maximum of 60 turns. If this still fails, we choose a non-optimal value of N_p to satisfy the constraints on the tuning capacitance, which results in higher magnetic field noise than predicted by Eq. (19). In fact, we find that the optimal magnetic field noise, with $N_p = \tilde{N}_p$, can only be achieved at frequencies between 30 kHz and 4 MHz. At lower frequencies, we require N_i to be several hundred to maintain $C_i \lesssim 0.1\ \mu\text{F}$. At higher frequencies, N_p decreases

---

[5] For a 5-μm wide input coil separated from the niobium SQUID washer by a 400 nm SiO insulating film, Mück and Clarke [24] estimate a capacitance per unit length of $C_0 \approx 0.6\ \text{nF/m}$. An $N = 4$ turn input coil wound around a 200 μm square washer SQUID has a length of ≈4 mm and a stripline capacitance of ≈3 pF, much less than the minimum tuning capacitance of 100 pF.
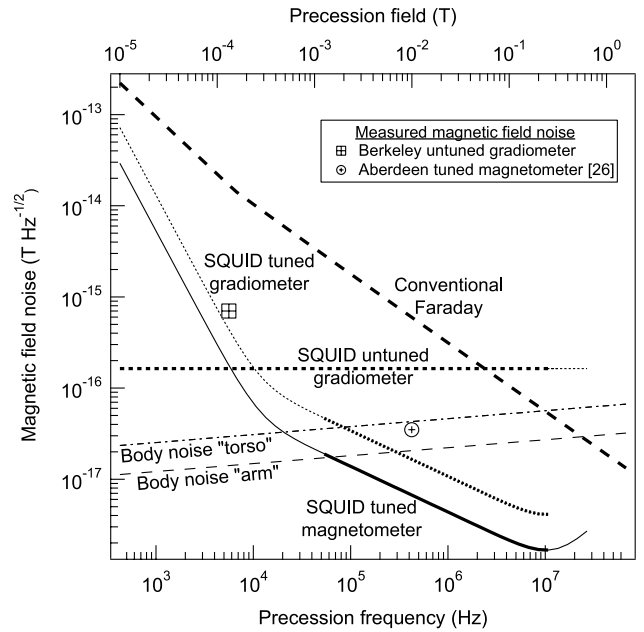

Fig. 7. Calculated magnetic field noise of tuned and untuned SQUID detectors and conventional Faraday detector compared to modeled sample noise. All gradiometers are second-order. Two experimentally measured values are also indicated. The curves are bold in frequency regimes where the theoretical magnetic field noise level is likely to be physically realizable. The noise is calculated for a 65 mm-diameter pickup coil as described in Section 2, and can be scaled for different geometries by changing the relevant parameters in Eqs. (10), (19), and (22).

below its optimal value to maintain $C_i \geqslant 100\ \text{pF}$. The constraints on C_i, N_i, and N_p set the maximum tuning frequencies of 11 MHz and 27 MHz for the gradiometer and the magnetometer, respectively.

Fig. 7 plots the magnetic field noise as a function of precession frequency for the constrained solution. The lowest tuned magnetometer noise of 0.002 fT Hz$^{-1/2}$ occurs at $\omega_0/2\pi = 10$ MHz and $N_p = 3$, while the lowest tuned gradiometer noise of 0.004 fT Hz$^{-1/2}$ occurs at $\omega_0/2\pi = 10$ MHz and $N_p = 1$. These detector noise values are substantially below the noise limits set by the sample noise and therefore cannot be exploited in practice. The higher inductance of the gradiometer requires more feedback damping to achieve the same bandwidth as the magnetometer; the increased feedback damping introduces additional noise. Surprisingly, the noise increases at frequencies above 10 MHz. This effect occurs because both the tuning capacitance and input coil turns have reached their constraints; as ω increases further, the circuit must be tuned by decreasing N_p. Since the current noise term in Eq. (14) goes as N_i^2/N_p^2 (recalling $M_i = \alpha^2 N_i L$), and N_i is held fixed by the constraint, the noise increases with increasing frequency.

4. Faraday detection

In conventional Faraday detection of MRI signals, the noise of the signal amplifier is negligible compared with the Nyquist noise in the room-temperature coil. For sim-

plicity, we consider a Faraday coil made from a single solid copper wire with cylindrical cross-section and radius $\phi = 3.25$ mm; the surface area is comparable to that of the copper-tape Faraday coils often used in high-field MRI. For a pickup coil with resistance R_i, inductance L_p, and area A_p connected to a tuning capacitor C_i and a matched semiconductor amplifier, the equivalent magnetic field noise at the resonant frequency $\omega_0 = (L_p C_i)^{-1/2}$ is

$$S_B^{1/2}(f) = \sqrt{4 k_B T R_i}/\omega_0 A_p, \qquad (20)$$

where $T = 298$ K is the temperature of the pickup coil. Since the current is confined to the skin depth $\delta = (2\rho/\mu_0 \omega_0)^{1/2}$ of a material with resistivity ρ, R_i depends on ω_0. The resistance of a solid wire pickup coil of radius a and wire radius ϕ is thus

$$R_i = \rho \frac{2\pi a}{2\pi \phi \delta} = \frac{a}{\phi} \sqrt{\frac{\mu_0 \rho \omega_0}{2}}. \qquad (21)$$

Since we assume a single turn solid-wire rf coil at $h = 8\phi$ above the conducting sample, we treat only the skin effect and not the proximity effect [25]. The resistance R_i results in a bandwidth $\Delta\omega = R_i/L_i$. For $\Delta\omega \geqslant \pi BW_{\text{det}}$, the magnetic field noise is given by substituting Eq. (21) into Eq. (20)

$$S_B^{1/2}(f) = \frac{1}{\omega_0^{3/4} A_p} \left(\frac{\mu_0 \rho}{2}\right)^{1/4} \sqrt{4 k_B T \frac{a}{\phi}}. \qquad (22)$$

which scales as $\omega_0^{-3/4}$; if additional resistance must be added to achieve the required bandwidth, $R_i = \Delta\omega L_i$ and $S_B^{1/2}(f)$ scales as ω_0^{-1}.

5. Comparison of modalities

Fig. 7 compares the magnetic field noise of a SQUID untuned second-order gradiometer, a SQUID tuned second-order gradiometer, a SQUID tuned magnetometer, and conventional Faraday detection to the sample noise calculated in Section 2.2 for a pickup loop with diameter $2a = 65$ mm at a distance $h = 25$ mm from a cylindrical sample. The optimal detection modality at a given precession frequency is the one with the lowest magnetic field noise. Comparing gradiometer performances at low frequencies, for $\omega_0/2\pi < 12$ kHz we find that SQUID untuned detection has the lowest magnetic field noise. Gradiometric SQUID untuned detection is likely to remain the more attractive modality up to around 50 kHz because tuned detection below that frequency involves gradiometers with more than 8 turns, which would be difficult to balance adequately. One could in principle use SQUID tuned magnetometers—which obviously do not involve balancing—at frequencies down to 12 kHz. In practice, however, these would require either a mu-metal enclosure—which is expensive—or substantial eddy-current shielding to reduce environmental noise. For example, in our own laboratory the noise near 12 kHz (between harmonics of 60 Hz) is typically 1 pT Hz$^{-1/2}$. Reducing this noise to (say) 0.1 fT

Hz$^{-1/2}$ would require an attenuation of 10^4. This could be achieved by means of an enclosure made of aluminum plate with a thickness of about 9 mm. Although perfectly feasible, in most applications such a shield would be undesirable. On the other hand, one would expect to be able to balance a single-turn gradiometer to better than 1 part in 10^4 [13], enabling it to operate unshielded. For these reasons, we believe an untuned gradiometer would be preferable to a tuned gradiometer at frequencies up to about 50 kHz.

The noise of the SQUID tuned gradiometer decreases with increasing frequency, approaching the sample noise at 100 kHz. Both SQUID tuned detection modalities have a noise minimum well below the sample noise at around 10 MHz, with increasing noise above this frequency. Examining the high-frequency regime, we see that for this particular geometry conventional Faraday detection is below the sample noise of the "torso" model above 10 MHz and the "arm" model above 25 MHz.

Fig. 7 also shows the experimentally measured magnetic field noise of two low-field systems: the Berkeley SQUID untuned second-order gradiometer and the SQUID tuned magnetometer of Seton et al. [26]. The untuned gradiometer has a single-turn pickup loop and operates at 5.6 kHz while the tuned magnetometer has a 29-turn pickup loop and operates at 425 kHz. In both cases, the measured noise is higher than the predicted value. In the case of the Berkeley gradiometer, the SQUID currently used in the system yields an intrinsic magnetic field noise of 0.6 fT Hz$^{-1/2}$, four times higher than that of the idealized SQUID used in our calculations. We note, however, that the flux-modulation scheme used in this system increases the noise by a factor of $\pi/2$, so that the predicted noise is in fact 0.25 fT Hz$^{-1/2}$. Thus, the experimental intrinsic noise is 2.4 times the predicted value, most likely due to parasitic resonances. The total measured system noise is 0.7 fT Hz$^{-1/2}$; the small additional contribution probably arises from external sources. Seton et al. attribute the excess noise in their measurements to dielectric losses, particularly in the cryostat.

The single-shot signal-to-noise ratio of an MRI experiment with voxel volume V_{voxel} is [27]

$$\text{SNR} = B_{\text{det}} \sqrt{T_{\text{acq}}}/S_B^{1/2}(f), \qquad (23)$$

where B_{det} scales linearly with V_{voxel} and B_p as shown in Eq. (3), and T_{acq} is the acquisition time. Fig. 8 plots the SNR of the 1 mm^3 voxel of water described in Section 2.1 as measured using the modalities shown in Fig. 7 with $T_{\text{acq}} = T_2 = 60$ ms. The polarizing field B_p is set to 100 mT for precession fields below 100 mT and to B_0 for precession fields above 100 mT. The noise from the "arm" model has been added in quadrature to the detector noise. As discussed above, prepolarized SQUID untuned detection is the optimal detection modality at frequencies below 50 kHz. Between 50 kHz and 4 MHz, prepolarized SQUID tuned detection with either a gradiometer or a
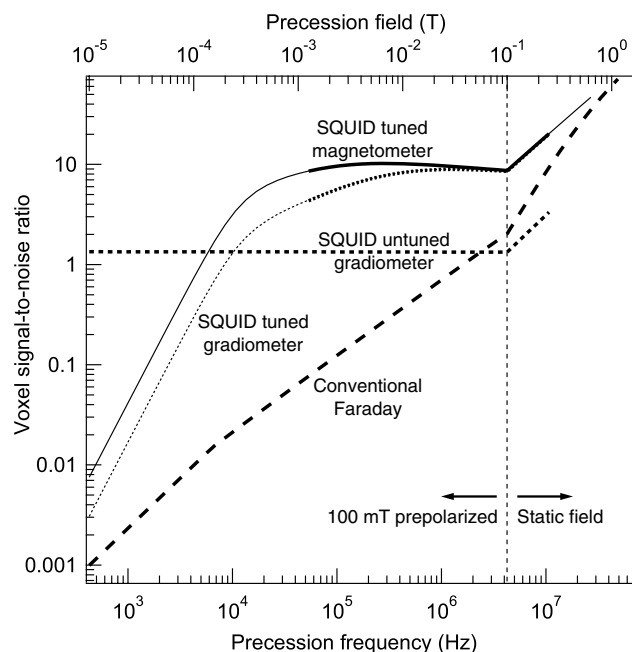
Fig. 8. Voxel signal-to-noise ratio comparison of the four different detection modalities with prepolarization at precession fields below 100 mT. Both gradiometers are second-order. Prepolarized SNR is plotted only for $B_0 < 100$ mT; above 100 mT the sample is polarized in the static precession field. The curves are bold in frequency regimes where the theoretical magnetic field noise level is likely to be physically realizable. The noise is calculated for a 65 mm-diameter pickup coil as described in Section 2, and can be scaled for different geometries by changing the relevant parameters in Eqs. (10), (19), and (22).

magnetometer is best. Going to higher frequencies, conventional Faraday detection will be the preferred modality as soon as the noise is limited by the sample noise. In our model, Faraday detection nears the ''arm'' model noise limit at 25 MHz. However, Fig. 8 overestimates the frequency at which realistic Faraday detection reaches the sample noise limit because it maintains the same 65-mm circular pickup coil geometry for all detectors. Free from the constraint that it must remain in a cylindrical cryostat, a Faraday coil at room temperature can be designed to couple more strongly to the sample than is possible with a superconducting coil. In this case, the distance from the sample to the coil can be decreased to 2 mm and the sample noise for the arm would be reached at about 7 MHz. However, this configuration increases sample noise by roughly a factor of 3, while the signal from the voxel of interest only doubles, resulting in an overall decrease in sample-noise-limited SNR. A saddle coil surrounding the human arm achieves twice the spatially averaged coupling of a circular pickup coil above the arm [27], so that Faraday detection with a saddle coil would reach the sample noise limit at 10 MHz. As described in the review by Darasse and Ginefri [7], the sample noise limit can be shifted to lower frequencies by using cooled copper coils or high-temperature superconducting (HTS) coils coupled to a semiconductor amplifier. In the model used in Ref. [7], a HTS coil with 65 mm diameter would reach the sample noise limit at

frequencies well below 100 kHz. However, at frequencies below ~2 MHz, the noise of the preamplifier would limit the available imaging bandwidth and this approach would not be practical [7]. Therefore, at frequencies below 2 MHz SQUID tuned detection remains the preferred modality.

Fig. 8 also reveals much about the potential of these detection modalities to acquire three-dimensional images of biological ($T_2 \sim 60$ ms) samples with $1 \times 1 \times 1$-mm^3 resolution. Comparing these methods to conventional Faraday detection without prepolarization, SQUID untuned detection with $B_p = 100$ mT achieves a SNR equivalent to conventional MRI at 70 mT, while prepolarized SQUID tuned detection at 400 kHz yields the same SNR as conventional MRI at 270 mT. One can see immediately that low-field SQUID detection will never surpass the SNR of conventional MRI at the 1.5 T clinical standard. Therefore, the potentially lower cost, more open geometry, and higher T_1-contrast of low-field MRI must compensate for its inferior SNR in any successful medical application.

6. Conclusions

Which low-field MRI detection modality and precession frequency should one choose? In principle, at frequencies below 12 kHz ($B_0 < 280$ μT), prepolarized SQUID untuned detection with a gradiometer is the best choice. In practice, although SQUID tuned detection has a lower intrinsic magnetic field noise above 12 kHz, external magnetic field noise and difficulties in manufacturing suitably large tuning capacitors and gradiometer inductances suggest that SQUID untuned detection remains the preferred modality up to approximately 50 kHz ($B_0 < 1.2$ mT). Since the SNR of this modality is independent of precession frequency, B_0 need only be strong enough to avoid the effects of concomitant gradients [28,29]. For all frequencies, the magnetic field noise of untuned detection is ~10 times the sample noise. SQUID untuned detection should only be used when the benefits of microtesla precession fields outweigh the lower SNR of this technique or to add MRI capabilities to existing SQUID-based biomagnetic detectors. For example, several authors [8,17] have suggested employing the multichannel SQUID arrays used in magnetoencephalography (MEG) as MRI detectors to create a combined MEG/MRI brain imaging system; the combined sensitivity of the hundreds of SQUIDs used in such systems would raise the SNR above that achieved with a single detector.

The magnetic field noise of the SQUID tuned gradiometer declines with increasing frequency until it reaches the sample noise at a crossover frequency ranging from 90 to 300 kHz depending on the sample size. The optimal precession frequency, which balances the marginal increase in SNR obtained by reducing the detector noise below the sample noise with the larger magnets required to produce the higher value of B_0, is probably about 200–400 kHz. In contrast, the magnetic field noise of conventional Faraday detection with a room-temperature copper coil (assuming the factor of two improvement in geometrical coupling

factor described in Section 5) reaches the sample noise at frequencies between 4 and 10 MHz, depending on the sample size. Above that transition it is the preferred modality. If one employs a cooled copper coil or a superconducting coil, Faraday detection with a conventional amplifier can be used down to 2 MHz [7].

In summary, we have shown that for imaging an object the size of the human arm each of the modalities discussed in this paper is superior over a particular range of precession fields: SQUID untuned detection at low fields, SQUID tuned detection at intermediate fields, and conventional Faraday detection at high fields. Lower precession fields generally give lower SNR, but each modality is capable of acquiring MR images in its ideal field range. The choice of modality therefore depends on the choice of precession field, which in turn is determined by factors such as T_1-contrast, cost, and openness.

Acknowledgments

Appendix A. Optimization of tuned input circuit

In this appendix we minimize the magnetic field noise of SQUID tuned detection with respect to the number of turns wound on the pickup coil. To optimize the number of turns on the input coil, we separate the intrinsic coil resistance R_i into eddy current losses R_e and dielectric losses R_d. As discussed in Section 2.2, the fluctuation-dissipation theorem indicates that R_e can also be modeled as magnetic field noise from the environment picked up at the detector. Since external magnetic field noise does not depend on N_p, R_e contributes a constant term to S_B that can be included in the sample noise but does not influence the optimal number of turns on the pickup coil. In contrast, R_d involves the tuning capacitor, the value of which is related to the inductance of the pickup loop and therefore depends on N_p.

The dielectric loss of a capacitor C_i can be described by its intrinsic quality factor $Q_0 = 1/\omega C_i R_d$, where ω is the angular frequency at which the loss is measured. Table 2 summarizes the quality factors measured in resonant circuits employing a variety of cryogenic capacitors. Since Seton obtained $Q_0 = 55,000$ in a 425 kHz SQUID tuned MRI system, we assume $Q_0 = 50,000$ for the superconduc-

Table 2
Intrinsic quality factor of resonant circuits (measured at 4.2 K unless noted)

Capacitor type	Capacitance	Frequency	Quality factor Q_0	Reference
Ceramic	0.1 and 1 μF	1–100 kHz	100–700[a]	[30]
Lead/mylar	125 nF	3.15 kHz	6400	[23]
Silver mica	11 pF	30 MHz	7320	[31]
Polystyrene	10 nF	425 kHz	42,000	[18]
Lead/PFTE	1.2 nF	425 kHz	55,500	[32]

[a] Measured at 73 K.

ting tuned circuits described in this paper [H. Seton, personal communication]. Fabrication constraints limit the maximum capacitance of such low-loss capacitors. Since one could almost certainly construct a lead/PFTE capacitor of at least 0.1 μF that would achieve $Q_0 > 10,000$, we conservatively assume a maximum capacitance of 0.1 μF.

Substituting $\omega = \omega_0$ and $R_i = R_d = \omega_0 L_T / Q_0$ into Eq. (17) yields

$$S_B(f) = \frac{1}{N_p^2 A_p^2} \left\{ \frac{4 k_B T L_T}{\omega_0 Q_0} + \frac{L_T^2 \Delta \omega^2}{\omega_0^2 M_i^2 V_\Phi^2} S_V(f) + M_i^2 S_J(f) \right\},$$
(24)

where $L_T = N_p^2 L_p + L_i$, $M_i^2 = \alpha^2 L L_i$, and $L_i = \alpha^2 N_i^2 L$ is the inductance of an input coil with N_i turns. Minimizing with respect to N_p gives the optimal number of pickup coil turns

$$\tilde{N}_p^2 = \frac{L_i}{L_p} \left[1 + \frac{4 k_B T \omega_0}{Q_0 S_V(f)} \frac{M_i^2}{L_i} \left(\frac{V_\Phi}{\Delta \omega} \right)^2 + \left(\frac{M_i^2}{L_i} \right)^2 \left(\frac{V_\Phi}{\Delta \omega} \right)^2 \frac{\omega_0^2 S_J(f)}{S_V(f)} \right]^{1/2}.$$
(25)

To estimate the order of magnitude of the expression in brackets in Eq. (25), we substitute $S_V(f) = 16 k_B T R$ and $S_J(f) = 11 k_B T / R$ and recall that $V_\Phi = R/L$ to obtain

$$\tilde{N}_p^2 L_p = L_i \left[1 + \frac{\alpha^2}{4 Q_0} \frac{\omega_0}{\Delta \omega} \frac{V_\Phi}{\Delta \omega} + \frac{11 \alpha^4}{16} \left(\frac{\omega_0}{\Delta \omega} \right)^2 \right]^{1/2}.$$
(26)

Since $\Delta \omega / V_\Phi = 9 \times 10^{-8}$, $\omega_0 / \Delta \omega \sim 10^3$, $\alpha \sim 1$, and $1/Q_0 = 2 \times 10^{-5}$ over the frequency range of interest, $\tilde{N}_p^2 L_p \approx 10^3 L_i$, and therefore $\tilde{L}_T \approx \tilde{N}_p^2 L_p \approx 10^3 L_i$.

Using this relation, we can now examine the relative magnitude of the terms in the minimized magnetic field noise spectral density, Eq. (24). Factoring out the first term yields

$$\tilde{S}_B(f) = \frac{4 k_B T \tilde{L}_T}{\tilde{N}_p^2 A_p^2 \omega_0 Q_0} \left\{ 1 + \frac{\tilde{L}_T (\Delta \omega)^2 Q_0}{4 k_B T \omega_0 M_i^2 V_\Phi^2} S_V(f) + \frac{\omega_0 Q_0 M_i^2}{4 k_B T \tilde{L}_T} S_J(f) \right\}.$$
(27)

and combining the substitutions above Eq. (26) with the approximation $\tilde{L}_T \approx 10^3 L_i$, we find

$$\tilde{S}_B(f) \approx \frac{4 k_B T \tilde{L}_T}{\tilde{N}_p^2 A_p^2 \omega_0 Q_0} \left\{ 1 + 4 \times 10^3 \frac{Q_0}{\alpha^2} \frac{\Delta \omega}{\omega_0} \frac{\Delta \omega}{V_\Phi} + \frac{11}{4} \times 10^{-3} Q_0 \alpha^2 \frac{\omega_0}{V_\Phi} \right\}.$$
(28)

Inserting the numerical values given above, we see that noise originating from loss in the capacitor overwhelms

the SQUID voltage and current noise. Eq. (28) can then be approximated by its first term

$$\tilde{S}_B(f) \approx \frac{4k_B T \tilde{L}_T}{\tilde{N}_p^2 A_p^2 \omega_0 Q_0} \approx \frac{4k_B T L_p}{A_p^2 \omega_0 Q_0}. \tag{29}$$

References

[1] R.W. Mair, M.I. Hrovat, S. Patz, M.S. Rosen, I.C. Ruset, G.P. Topulos, L.L. Tsai, J.P. Butler, F.W. Hersman, R.L. Walsworth, He-3 lung imaging in an open access, very-low field human magnetic resonance imaging system, Magn. Reson. Med. 53 (2005) 745.

[2] M. Mößle, W.R. Myers, S.-K. Lee, N. Kelso, M. Hatridge, A. Pines, John Clarke, SQUID-detected in vivo MRI at microtesla magnetic fields, IEEE T. Appl. Supercon. 15 (2005) 757.

[3] C.H. Tseng, G.P. Wong, V.R. Pomeroy, R.W. Mair, D.P. Hinton, D. Hoffmann, R.E. Stoner, F.W. Hersman, D.G. Cory, R.L. Walsworth, Low-field MRI of laser polarized noble gas, Phys. Rev. Lett. 81 (1998) 3785.

[4] M. Mößle, S.-I. Han, W.R. Myers, S.-K. Lee, N. Kelso, M. Hatridge, A. Pines, John Clarke, SQUID-detected microtesla MRI in the presence of metal, J. Magn. Reson. 179 (2006) 146.

[5] R.D. Venook, N.I. Matter, M. Ramachandran, S.E. Ungersma, G.E. Gold, N.J. Giori, A. Macovski, G.C. Scott, S.M. Conolly, Prepolarized magnetic resonance imaging around metal orthopedic implants, Magn. Reson. Med. 56 (2006) 177.

[6] S.-K. Lee, M. Mößle, W. Myers, N. Kelso, A.H. Trabesinger, A. Pines, John Clarke, SQUID-detected MRI at 132 μT with T_1-weighted contrast established at 10 μT–300 μT, Magn. Reson. Med. 53 (2005) 9.

[7] L. Darrasse, J.-C. Ginefri, Perspectives with cryogenic RF probes in biomedical MRI, Biochimie 85 (2003) 915.

[8] R. McDermott, S.-K. Lee, B. ten Haken, A.H. Trabesinger, A. Pines, John Clarke, Microtesla MRI with a superconducting quantum interference device, PNAS 101 (2004) 7857.

[9] D.I. Hoult, D.E. Richards, The signal-to-noise ratio of the nuclear magnetic resonance experiment, J. Magn. Reson. 24 (1976) 71.

[10] M. Decorps, P. Blondet, H. Reutenauer, J.P. Alebrand, An inductively coupled, series-tuned NMR probe, J. Magn. Reson. 65 (1985) 100.

[11] B.H. Suits, A.N. Garroway, J.B. Miller, Surface and gradiometer coils near a conducting body: the lift-off effect, J. Magn. Reson. 135 (1998) 373.

[12] S. Gabriel, R.W. Lau, C. Gabriel, The dielectric properties of biological tissues: II. Measurements in the frequency range 10 Hz to 20 GHz, Phys. Med. Biol. 41 (1996) 2251.

[13] J. Clarke, A. Braginski (Eds.), The SQUID Handbook, Vol. 1, Wiley-VCH, Weinheim, 2003.

[14] C. Tesche, J. Clarke, dc SQUID: Current Noise, J. Low Temp. Phys. 37 (1979) 397.

[15] M. Mück, C. Welzel, John Clarke, Superconducting quantum interference device amplifiers at gigahertz frequencies, Appl. Phys. Lett. 82 (2003) 3266.

[16] T. Ryhänen, H. Seppä, R. Ilmoniemi, J. Knuutila, SQUID magnetometers for low-frequency applications, J. Low Temp. Phys. 76 (1989) 287.

[17] A.N. Matlachov, P.L. Volegov, M.A. Espy, J.S. George, R.H. Kraus Jr., SQUID detected NMR in microtesla fields, J. Magn. Reson. 170 (2004) 1.

[18] H.C. Seton, D.M. Bussell, J.M.S. Hutchison, D.J. Lurie, Use of a DC SQUID receiver preamplifier in a low field MRI system, IEEE T. Appl. Supercon. 5 (1995) 3128.

[19] H.C. Seton, J.M.S. Hutchison, D.M. Bussell, Gradiometer pick-up coil design for a low field SQUID-MRI system, Magn. Reson. Mater. Phy. 8 (1999) 116.

[20] D. Shoenberg, Superconductivity, Cambridge University Press, Cambridge, 1962.

[21] J. Clarke, SQUID concepts and systems, in: H. Weinstock, M. Nisenoff (Eds.), Superconducting Electronics, Springer, Berlin, 1989, pp. 87–148.

[22] J.M. Martinis, John Clarke, Signal and noise theory for a DC SQUID amplifier, J. Low Temp. Phys. 61 (1985) 227.

[23] M.B. Simmonds, W.A. Fertig, R.P. Gifford, Performance of a resonant input SQUID amplifier system, IEEE Trans. Mag. 15 (1979) 478.

[24] M. Mück, John Clarke, The superconducting quantum interference device microstrip amplifier: computer models, J. Appl. Phys. 88 (2000) 6910.

[25] F.E. Terman, Radio Engineer's Handbook, first ed., McGraw-Hill, New York, 1943, pp. 77-80.

[26] H.C. Seton, J.M.S. Hutchison, D.M. Bussell, Liquid helium cryostat for SQUID-based MRI receivers, Cryogenics 45 (2005) 348.

[27] W.R. Myers, Potential applications of microtesla magnetic resonance imaging detected using a superconducting quantum interference device, PhD thesis, University of California, Berkeley (2006).

[28] W.R. Myers, M. Mößle, John Clarke, Correction of concomitant gradient artifacts in experimental microtesla MRI, J. Magn. Reson. 177 (2005) 274.

[29] C.A. Meriles, D. Sakellariou, A.H. Trabesinger, Theory of MRI in the presence of zero to low magnetic fields and tensor imaging field gradients, J. Magn. Reson. 182 (2006) 106.

[30] A. Hammoud, S. Geerber, R.L. Patterson, T.L. MacDonald, Performance of surface-mount ceramic and solid tantalum capacitors for cryogenic applications, 1998 Annual Report Conference on Electrical Insulation and Dielectric Phenomena, IEEE, vol. 2 (1998) 572.

[31] C. Hilbert, John Clarke, T. Sleator, E.L. Hahn, Nuclear quadrupole resonance detected at 30 MHz with a dc superconducting quantum interference device, Appl. Phys. Lett. 47 (1985) 637.

[32] H.C. Seton, J.M.S. Hutchison, D.M. Bussell, A 4.2 K receiver coil and SQUID amplifier used to improve the SNR of low-field magnetic resonance images of the human arm, Meas. Sci. Technol. 8 (1997) 198.